ORNL/TM-7810

OAK RIDGE NATIONAL LABORATORY

UNION CARBIDE

Ferrite Morphology and Variations in Ferrite Content in Austenitic Stainless Steel Welds

S. A. David
S. E. Hanzelka
C. P. Haltom

OAK RIDGE NATIONAL LABORATORY
CENTRAL RESEARCH LIBRARY
CIRCULATION SECTION
4500N ROOM 175
LIBRARY LOAN COPY
DO NOT TRANSFER TO ANOTHER PERSON
If you wish someone else to see this report, send in name with report and the library will arrange a loan.

OPERATED BY
UNION CARBIDE CORPORATION
FOR THE UNITED STATES
DEPARTMENT OF ENERGY

ORNL/TM-7810
Distribution
Category UC-25

Contract No. W-7405-eng-26

METALS AND CERAMICS DIVISION

FERRITE MORPHOLOGY AND VARIATIONS IN FERRITE CONTENT IN AUSTENITIC STAINLESS STEEL WELDS

S. A. David, S. E. Hanzelka, and C. P. Haltom

Date Published: July 1981

NOTICE: This document contains information of a preliminary nature. It is subject to revision or correction and therefore does not represent a final report.

OAK RIDGE NATIONAL LABORATORY
Oak Ridge, Tennessee 37830
operated by
UNION CARBIDE CORPORATION
for the
DEPARTMENT OF ENERGY

LOCKHEED MARTIN ENERGY RESEARCH LIBRARIES

3 4456 0452095 3

CONTENTS

ABSTRACT 1
INTRODUCTION 1
EXPERIMENTAL PROCEDURE 4
Welding 4
Melting and Casting 5
Microstructural Characterization 5
WELD METAL MICROSTRUCTURE AND FERRITE MORPHOLOGY 6
Type I — Vermicular Morphology 10
Type II — Lacy Morphology 10
Type III — Acicular Morphology 11
Type IV — Globular Morphology 11
VARIATIONS IN FERRITE CONTENT 13
SHAPE INSTABILITY OF FERRITE IN THE WELD 21
CONCLUSIONS 23
ACKNOWLEDGMENTS 24
REFERENCES 24

FERRITE MORPHOLOGY AND VARIATIONS IN FERRITE CONTENT IN AUSTENITIC STAINLESS STEEL WELDS

S. A. David, S. E. Hanzelka, and C. P. Haltom

ABSTRACT

Four distinct ferrite morphologies have been identified in type 308 stainless steel multipass welds: vermicular, lacy, acicular, and globular. The first three ferrite types are related to transformations following solidification and the fourth is related to the shape instability of the residual ferrite.

An earlier study showed that most of the ferrite observed in austenitic stainless steel welds containing a duplex structure may be identified as residual primary ferrite resulting from incomplete $\delta \rightarrow \gamma$ transformation during solidification and/or residual ferrite after Widmanstätten austenite precipitation in primary ferrite. These modes of ferrite formation can be used to explain observed ferrite morphologies in austenitic stainless steel welds.

Variations in ferrite content within the weld were related to weld metal composition, ferrite morphology, and dissolution of ferrite resulting from thermal cycles during subsequent weld passes. An investigation of the type 308 stainless steel filler metal solidified over cooling rates ranging from 7 to 1600°C/s showed that the cooling rate of the weld metal within the freezing range of the alloy affects the amount of ferrite in the microstructure very little. However, the scale of the solidification substructure associated with various solidification rates may influence the ferrite dissolution kinetics.

INTRODUCTION

Though several studies[1–3] show that a certain amount of ferrite should be present in austenitic stainless steel welds to prevent hot cracking, the mechanism is not well understood. Although several researchers have proposed 3 to 5 ferrite number (FN) as the required amount to prevent hot cracking, the true amount of ferrite present or required during the critical stage of weld metal solidification is unknown.

Ferrite also influences the strength and corrosion behavior of austenitic stainless steel welds in various ways.[4-8] For a given composition ferrite may be present in various amounts and in different morphologies within the weld, depending on the welding processes and parameters. Recently Devine[9] found that the amount and morphology of ferrite influence the sensitization behavior of duplex stainless steel. In particular, for a given carbon content, a critical amount and distribution of $\delta-\gamma$ boundary area exist above which the alloy is immune to sensitization. It can therefore be seen that ferrite morphology plays an important role in weld behavior.

Ferrite morphology and variations in ferrite content within a weld have received very little attention.[10,11] Recently, Suutala, Takalo, and Moisio[12,13] referred to three types of weld metal microstructures based on the composition and solidification mode. Though their classification may adequately describe the general microstructures, it does not refer to distinct ferrite morphologies and other forms of ferrite often observed in weld metal microstructures. Lai and Townsend[14] have noted that the vermicular and needlelike ferrite morphologies described by Takalo and Moisio[15] are the same. For austenitic stainless steel welds containing duplex structure, the term "typical microstructure" is often misleading. Generally the weld metal has no single representative microstructure but rather is a combination of microstructures with various ferrite forms influenced by such factors as local variations in cooling rate and composition. Hence, detailed observation and classification of ferrite in welds based on its distinct shape and form are needed. In addition to the influence of composition on the ferrite morphology, effects of cooling rate and the thermal excursions during a multipass weld commonly influence ferrite content in austenitic stainless steel welds. The variation in ferite content has often been attributed to the inadequacies of the present ferrite measuring devices. In addition to the problems associated with the accuracy of ferrite measurement techniques, a number of other factors contribute to the observed variations in measured ferrite content within the weld metal: composition, ferrite morphology, dissolution and/or transformation of ferrite due to thermal cycles, and cooling

rate. The composition of the weld metal expressed as a ratio of chromium to nickel equivalents (Cr_{eq}/Ni_{eq})* is one of the major factors determining the ferrite content of the weld. The Schaeffler[16] constitution diagram originally provided a method for calculating as-welded ferrite content. This constitution diagram was further modified by DeLong and others[17,18] to take into account the austenitizing effect of nitrogen. It should be pointed out that the ferrite in austenitic stainless steel weld metal is a nonequilibrium phase and that any lack of good correlation between the composition and ferrite content could result from a number of other factors. For one, the ferrite morphology as influenced by the mode of solidification and subsequent solid state transformations may also contribute to the variations in measured ferrite content within the weld. A relationship between ferrite content and weld metal microstructure has been observed.[12] However, the thermal cycles to which some of the initial weld passes are subjected during a multipass weld are another factor that could contribute to the observed variations within the weld metal. Since the ferrite in the weld metal is not an equilibrium structure, thermal cycling could dissolve it, thus bringing about a change in ferrite content of the weld from region to region. In addition the ferrite could transform in part to a nonmagnetic sigma phase. The effect of cooling rate on ferrite content has been demonstrated[4] by the excessive amount of ferrite produced in a commercial wrought type 347 alloy that was cooled rapidly. This alloy would normally have had little or no ferrite. In addition, little or no ferrite has been produced in rapidly cooled electron-beam-welded type 312 stainless steel. Slower cooling rates normally produce well over 20 vol % ferrite in this alloy. Similar observations have been made by David and Vitek[19] during high-power laser welding of type 308 stainless steel at welding speeds exceeding 24 mm/s. It should be pointed out that these cooling rates represent extremes. Producing metastable structures under extremely rapid or slow cooling is not very unusual.[20]

---

*Cr_{eq} = Cr + Mo + 1.5 Si + 0.5 Nb, and Ni_{eq} = Ni + 30 C + 0.5 Mn + 30 N, where the symbols represent the weight percentages of the elements. The nitrogen content of the weld metal was analyzed to be 0.04 wt %.

Our purpose was to identify and classify different ferrite morphologies in austenitic stainless steel welds and offer possible explanations as to their origins. In addition, we identified various factors that influenced the ferrite content of the weld metal.

EXPERIMENTAL PROCEDURE

Welding

Two multipass welds were deposited on 25-mm-thick (1-in.) type 304L stainless steel plate [0.019 C, 1.75 Mn, 0.029 P, 0.006 S, 0.63 Si, 18.55 Cr, 10.0 Ni, and balance Fe (wt %)] containing a single-V-groove butt joint. One of the two welds was made with joint surfaces buttered with the weld metal and the other without buttering. The welds were made with type 308 stainless steel filler metal [0.016 C, 0.35 Si, 0.004 S, 0.029 P, 1.95 Mn, 9.76 Ni, 20.14 Cr, and balance Fe (wt %)] by the hot wire gas tungsten arc process (GTA). The welding parameters are given in Table 1.

Table 1. Welding parameters

Welding Arc	
Electrode	4.1 mm (0.16 in.) long, 2% ThO_2–W
Electrode top	30° included angle with 1.9 mm (0.075 in.) flat
Shielding gas	75 He–25 Ar (vol %), 2.4×10^{-3} m^3/s (30 cfh)
Backup gas	Argon
Arc voltage	15 V
Current	350 A dcsp
Hot Wire	1.1 mm (0.045 in.) long
Voltage	7 V
Current	80 A

Each weld consisted of eight passes. Samples for FN measurements were taken after each pass, and the average ferrite number of the root pass was measured after each pass. Ferrite number was measured by magnetic permeability with a Magne-gage instrument. The FN was measured in accordance with AWS Specification A4-2-74, "Calibrating Magnetic Instruments to Measure the δ-Ferrite Content of Austenitic Stainless Steel Weld Metal."

Melting and Casting

To characterize structures resulting from extreme variations in solidification conditions, additional specimens were prepared by several alternate techniques. Samples were cooled at estimated[21] rates ranging from 12 to 65°C/s by drop casting arc-melted type 308 stainless steel filler metal (of composition described earlier) into a water-cooled copper mold described elsewhere[22]. In addition, two other cooling rates, one estimated[23] to be 1600°C/s and the other measured to be 7°C/s, were obtained by quenching 2- to 3-mm-diam (0.08–0.1-in.) filler metal droplets in iced water and casting a 50-mm-diam (2-in.) bar into a graphite mold, respectively.

Microstructural Characterization

Standard metallographic techniques for austenitic stainless steels were used for microstructural analysis. The samples were etched with a solution containing five parts concentrated HCl to one part concentrated HNO_3. The secondary dendrite arm spacings were measured with a filar eyepiece. To investigate the ferrite morphology, small volume elements containing representative ferrite morphologies were cut from the weld and polished on three orthogonal planes.

Foils of weld metal for electron microscopic analysis were electropolished with a dual-jet polishing apparatus and a solution of 10 vol % perchloric acid in methanol. The samples were polished at −10°C (17°F) with 55 V dc. To determine if any precipitate particles were in the weld metal, electrolytic extractions were performed on the weld.

The extracted precipitate particles were then analyzed by x-ray diffraction. The details of the extraction and x-ray procedures are reported elsewhere.[24]

WELD METAL MICROSTRUCTURE AND FERRITE MORPHOLOGY

Macroscopic views of cross sections from the two welds are shown in Fig. 1. A wide variety of microstructures were observed at various

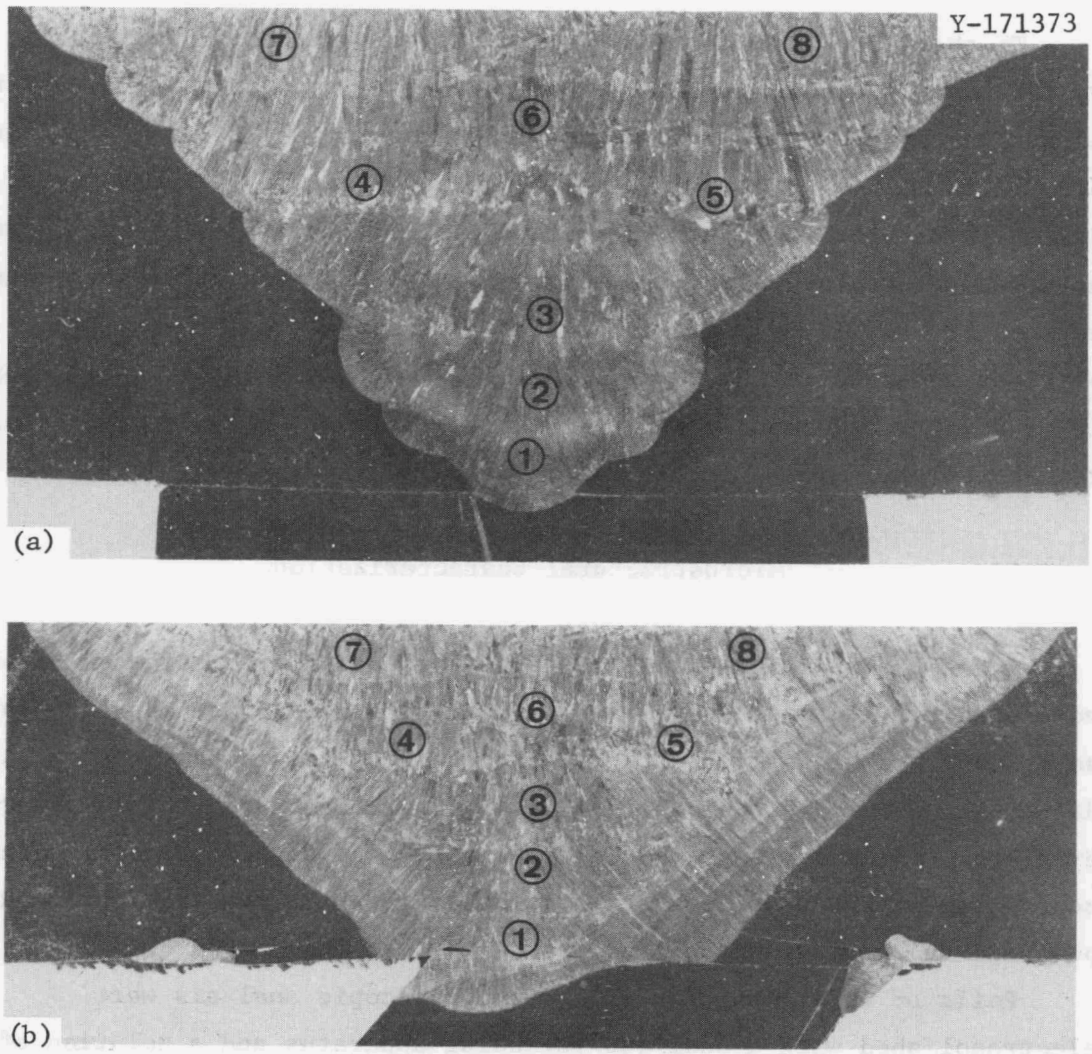

Fig. 1. Cross sections of type 308 stainless steel multipass welds. Base plate is 25 mm (1 in.) thick. (a) With unbuttered joint surfaces. (b) With buttered joint surfaces.

locations within the multipass welds. The microstructure is duplex, with ferrite being the minor phase distributed in various forms in an austenite matrix. To a great extent the solidification behavior and subsequent solid state transformations that occur within the weld metal on cooling control the microstructural characteristics of the weld metal. Suutala and co-workers[12] have described some of these microstructural features, relating them to different modes of solidification. An earlier study[25] involving thermal analysis and interrupted solidification experiments revealed that the solidification sequences in type 308 stainless steel filler metal include primary crystallization of δ-ferrite with subsequent envelopment by austenite. From the point of complete envelopment, further transformations $L \rightarrow \gamma$ and $\delta \rightarrow \gamma$ proceed at the δ-L and γ-δ interfaces. Further, as the sample cools to a temperature below that of the solidus, the transformation at the γ-L interface goes to completion, leaving behind a skeletal network of untransformed δ-ferrite along the cores of the primary and secondary dentrite arms. This residual ferrite has been shown to be enriched in chromium, which makes it very stable (Fig. 2). However, primary ferrite with a lower average chromium concentration of approximately 24 to 25 wt % may transform to Widmanstatten austenite and ferrite during rapid cooling. During the above transformations extensive solute redistribution occurs by diffusion. These two modes of ferrite formation may be used to explain the various ferrite morphologies observed in austenitic stainless steel welds.

From the orthogonal sectioning of the volume elements extracted from various locations within the multipass weld with buttered joint surfaces, we have identified four distinct types of ferrite morphologies: type I — vermicular, type II — lacy, type III — acicular, and type IV — globular. Figure 3 shows three-dimensional views of these four ferrite forms. As stated earlier, austenitic stainless steel welds containing a duplex structure have no single representative microstructure. All four morphologies shown in Fig. 3 were observed in the same multipass weld made with type 308 stainless steel filler metal of constant $Cr_{eq}/Ni_{eq} \approx 1.66$. Also, the literature often characterizes ferrite morphology as continuous

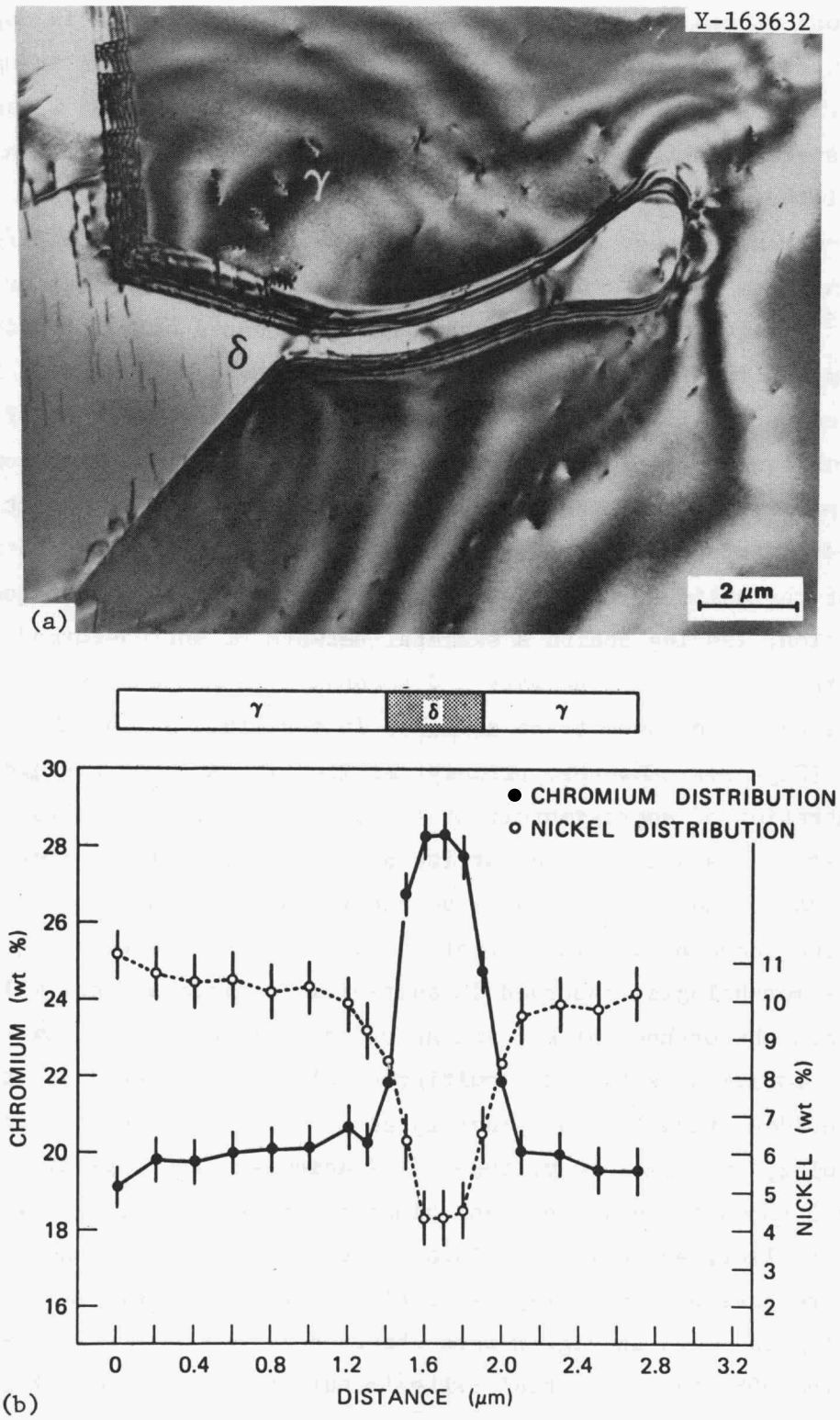

Fig. 2. Scanning transmission electron microscopic analysis of ferrite in the gas tungsten arc bead-on-plate weld. (a) Transmission electron micrograph. (b) Solute profiles across the ferrite.

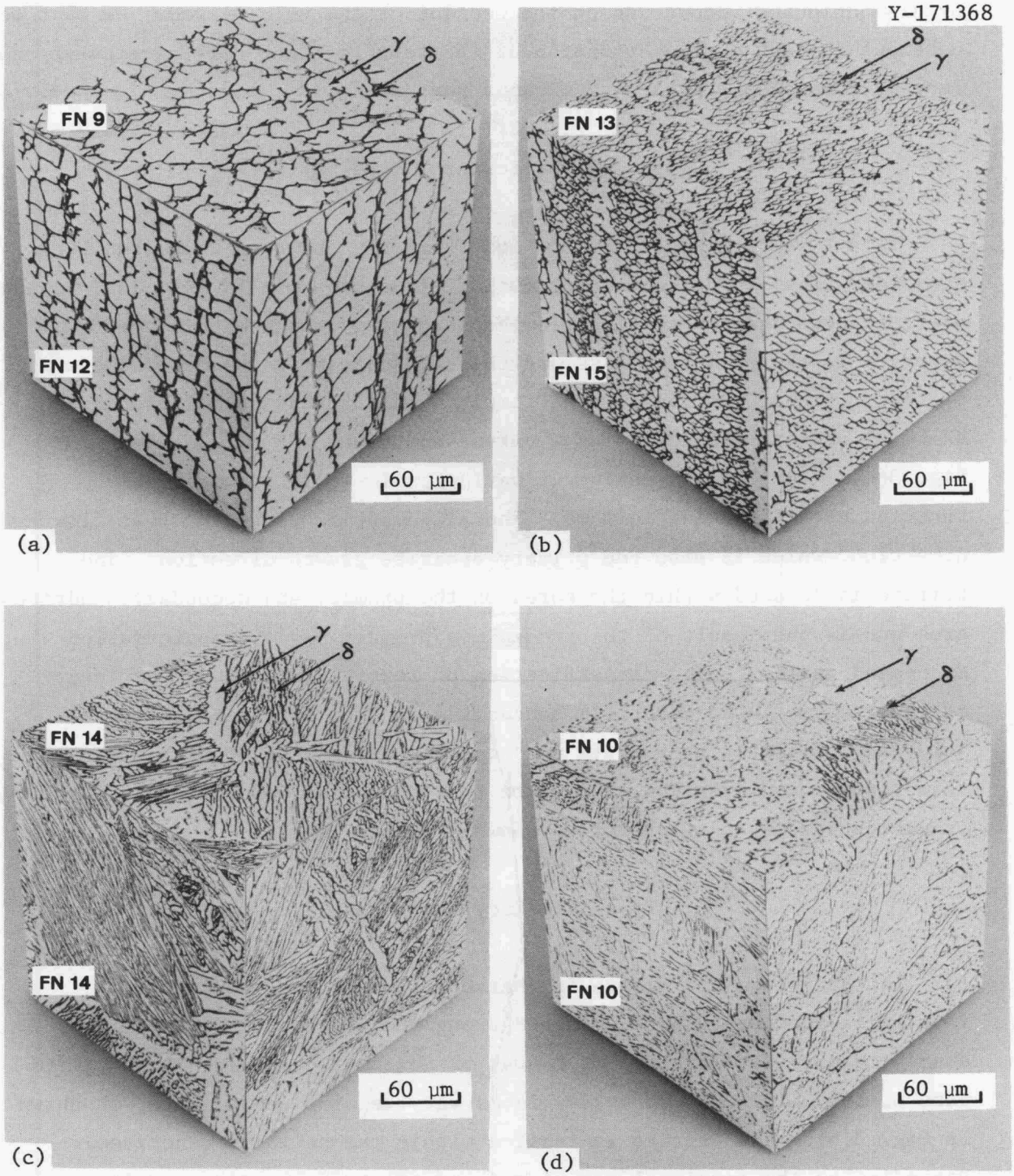

Fig. 3. Three-dimensional composite micrographs of various ferrite morphologies in type 308 stainless steel multipass weld. (a) Type I, vermicular. (b) Type II, lacy. (c) Type III, acicular. (d) Type IV, globular.

or discontinuous, depending on the section of the weld viewed. We must be cautious in such characterization of the ferrite since only vermicular and lacy morphologies approach continuous shapes.

Type I — Vermicular Morphology

This type ferrite is the one most commonly observed in austenitic stainless steel welds containing duplex structure with FN 5 to 15. In the present investigation this particular morphology was predominantly observed in the weld root pass and the two subsequent passes. Depending on the sectional cut viewed, the ferrite could appear as an aligned skeletal network (FN 12) or as a curved soft form (FN 9), as shown in Fig. 3(a). Further discussion of variation in ferrite number as a function of orientation follows. The alignment is along the heat flow direction, which is also the primary dendrite growth direction. The ferrite is located within the cores of the primary and secondary dendrite arms and is the result of the incomplete primary $\delta \rightarrow \gamma$ transformation discussed earlier. The classification of ferrite located at the intercellular or cellular dendritic boundaries in type 310 stainless steel welds as vermicular by Suutala and co-workers[12] may be debatable since this ferrite would seldom tend to be continuous and vermicular. Often it is discontinuous and globular as shown later.

Type II — Lacy Morphology

The lacy form of ferrite is characterized by long columns of interlaced ferrite network oriented along the growth direction in an austenite matrix. This structure was predominantly present in the third pass of the weld. The structure looks very regular and aligned, as shown in Fig. 3(b). The ferrite is located within the cellular dendrites. Depending on the sectional cut viewed and the corresponding ferrite measurement, the duplex structure showed a FN 13 or 15. The origin of this ferrite morphology is likely to be the transformation of primary δ-ferrite cells to Widmanstätten austenite and ferrite, as discussed earlier.

Type III — Acicular Morphology

The acicular morphology is characterized by the random arrangement of needlelike ferrite distributed in an austenite matrix, as shown in Fig. 3(c). This type structure was predominantly present in the sixth and crown passes of the weld (passes 7–8). Unlike the two morphologies described earlier, the structure here has no directionality and also does not seem to conform to the solidification substructure in any way. The average FN of the structure is 13. A similar structure has been observed in filler metals types 318 (ref. 12) and 312 stainless steel[26] with a high Cr_{eq}/Ni_{eq} ratio. This ferrite morphology is typical of weld metals with $Cr_{eq}/Ni_{eq} > 2$. The presence of this particular ferrite form in the present weld ($Cr_{eq}/Ni_{eq} = 1.66$) could be attributed to local variations in composition, mainly macrosegragation. It should be pointed out that the last few passes were made by oscillating the welding head laterally from one side wall to the other to cover the width of the weld. Such a motion, in addition to giving a complex puddle shape, would enhance turbulent fluid flow in the weld puddle, which could promote melting and/or breaking off of the chromium-rich cellular dendrites.[27] Such events in turn could bring about a change in liquid composition and the mode of solidification to $L \rightarrow L + \delta \rightarrow \delta$ and grain structure in localized regions. Further, the structure has its origin in the low-temperature transformation of primary ferrite that formed during solidification to austenite and ferrite. The austenite appears to have nucleated at the grain boundaries and grown inside the grains by an acicular mechanism.

Type IV — Globular Morphology

The globular form is characterized by ferrite in the form of globules randomly distributed in a matrix of austenite, as shown in Fig. 3(d). As in the acicular form, the structure has no directionality and is not related to the overall solidification substructure. It is commonly observed in weld passes 4, 5, and 6 of the multipass weld. Along with passes 1 through 3, these passes were subjected to thermal cycling during

welding. This structure typically has an average FN of 10. The structure appears to have its origin in the thermal instability of any of the other types of ferrite, particularly the acicular form. The thermal cycles to which some of the weld passes are subjected in a multipass weld seem to bring about shape instabilities of the type described later. As a result of the shape instability, the long thin ferrite needles in the acicular structure and the interlaced ferrite in the lacy structure could break down into small disconnected globules. Figure 4 shows such a microstructural instability in the acicular morphology of ferrite. In

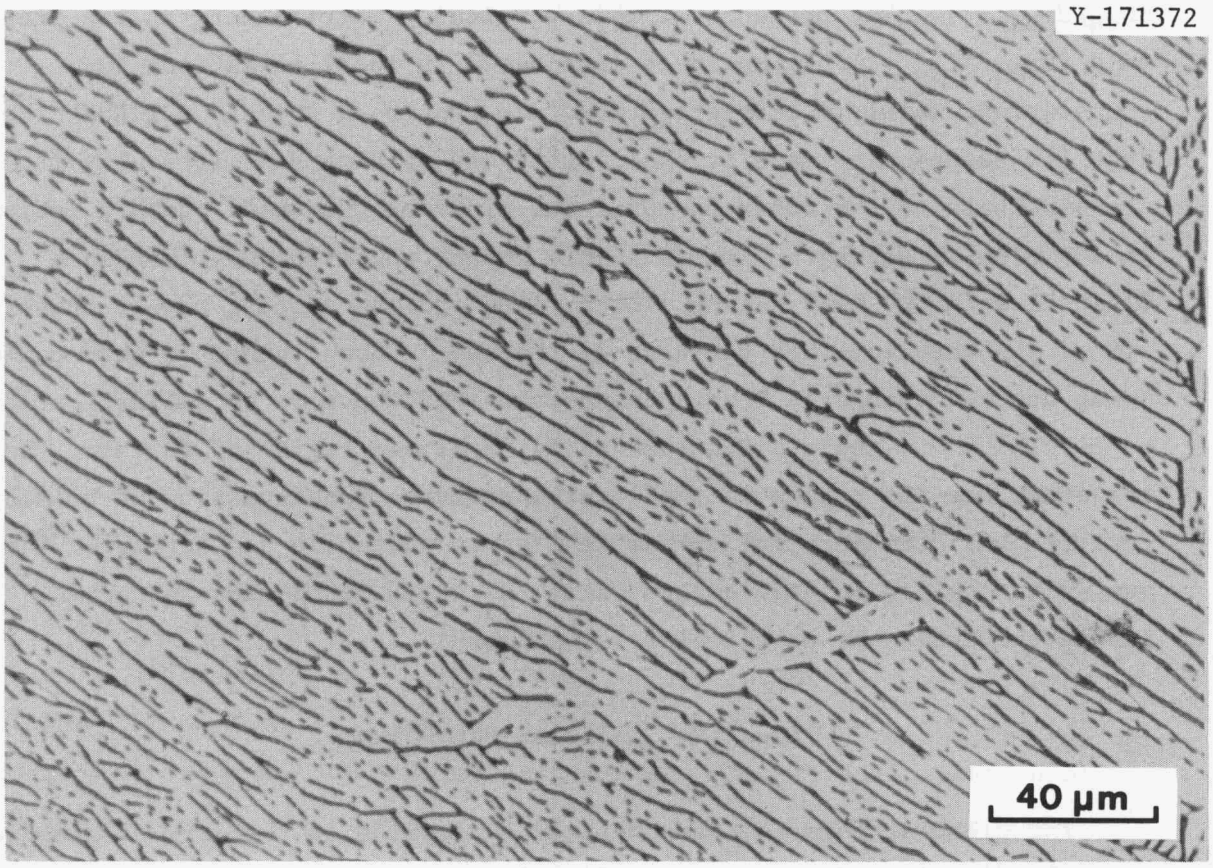

Fig. 4. The breakdown of acicular ferrite to globular ferrite in type 308 stainless steel multipass weld.

addition to the thermal effects, stress during thermal cycling could intensify microstructural instability, which is very common in materials containing duplex structures, particularly aligned eutectics.[28] The globular morphology of ferrite may also be seen in type 310 stainless steel welds [0.11 C, 1.64 Mn, 0.014 P, 0.009 S, 26.73 Cr, 21.15 Ni, and balance Fe (wt %)], where a very low volume fraction of ferrite in globular form may be present in the intercellular or interdendritic region, as shown in Fig. 5. The ferrite here is very discontinuous and forms as a result of the continuous enrichment of chromium in the liquids ($K_{Cr}^{\gamma L} < 1$)* during solidification.

VARIATIONS IN FERRITE CONTENT

As stated earlier, a number of factors such as composition, ferrite morphology, ferrite dissolution and/or transformation, and cooling rate may influence the amount of ferrite present within the weld deposit. Any such variation in ferrite content from location to location within the weld may influence its mechanical and chemical behavior.

Figure 6 shows the variation in the root pass FN within the two welds in our study. In weld 1 (top curve) the base-metal joint surfaces were buttered with the weld metal, while in weld 2 (bottom curve) the base metal joint surfaces were not buttered. The average FNs of the root pass deposit in welds 1 and 2 are 13 and 8, respectively. The lower FN of the root pass deposit in weld 2 is attributable to the weld metal dilution with the base metal and hence indicates a change in the weld metal composition. In practice the extent of dilution depends on the welding process and procedure variables such as current, travel speed, welding technique, joint design, and material thickness. The further decrease in

---

*Equilibrium partition ratio $K_{Cr}^{\gamma L} = C_{Cr}^{\gamma}/C_{Cr}^{L}$, where C_{Cr}^{γ} and C_{Cr}^{L} are The chromium concentrations in austenite and liquid given by the tie line at a particular temperature.

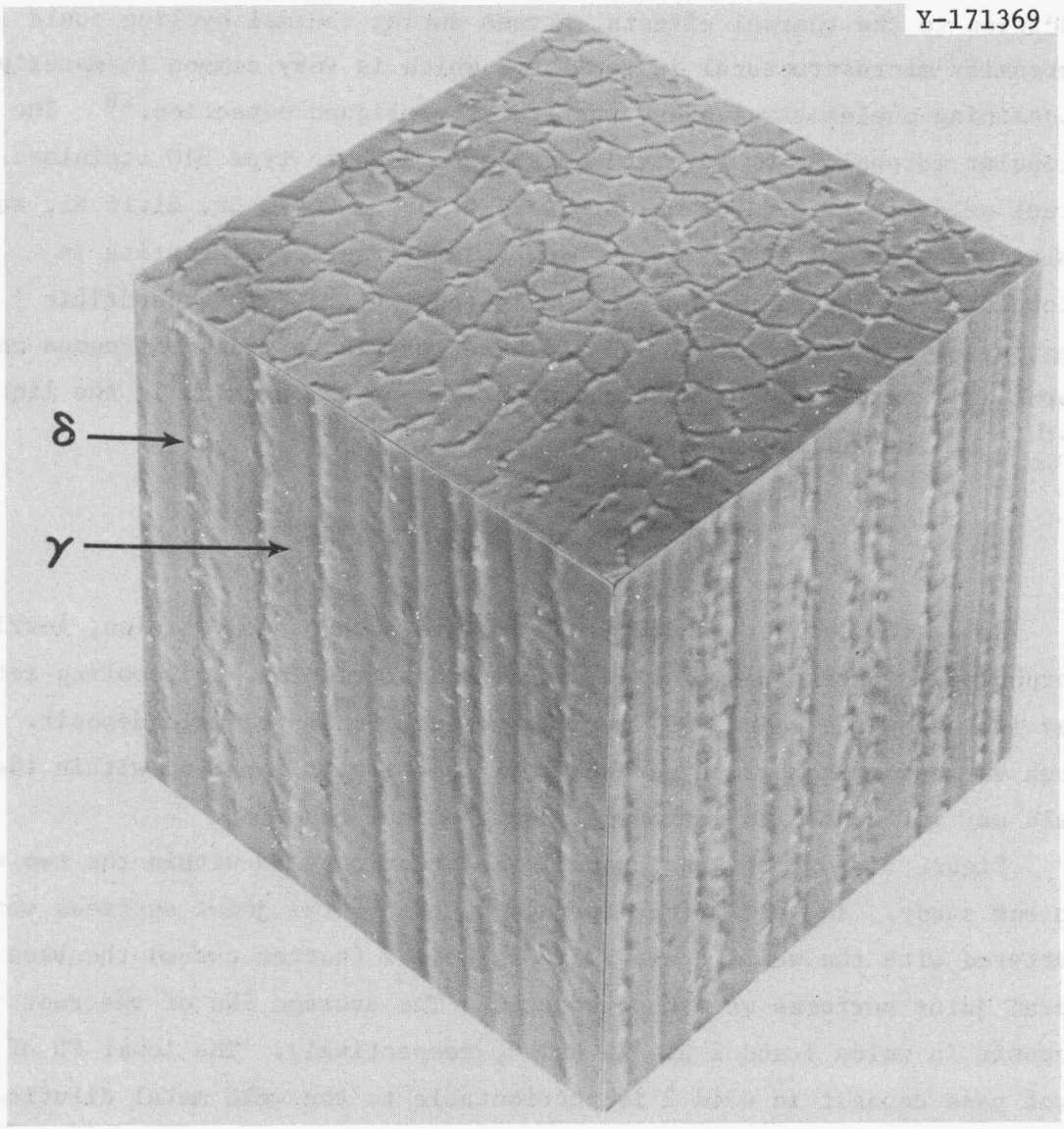

Fig. 5. Three-dimensional composite micrograph showing cellular structure in type 310 stainless steel weld metal with ferrite in globular from located in the intercellular regions.

FN of the root pass deposit in both welds results from the dissolution of ferrite from the thermal effects to which the root pass is subjected during a multipass weld. The dissolution of ferrite will be discussed in great detail later in this paper.

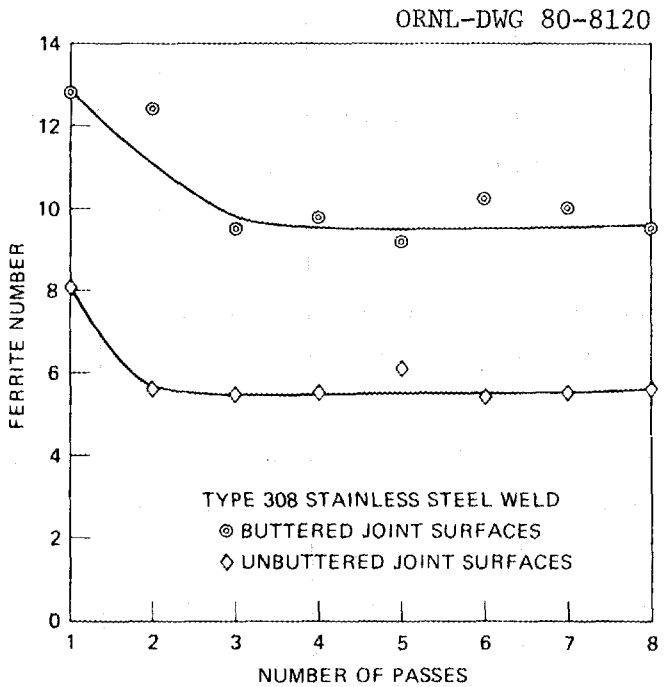

Fig. 6. Variations in root pass ferrite number with subsequent passes in welds made with buttered and unbuttered joint surfaces.

In addition to the observed thermal effects during subsequent passes on the FN of the root pass, variations in FN were observed in both welds within a cross section of the bead, along the length and width of the weld, and from bead to bead. Generally the FN increased from the root pass to the crown pass. The ferrite content within the weld at various locations varied from 5 to 14 and 9 to 13 for the welds with unbuttered and buttered joint surfaces, respectively. Some of these variations are attributable to dilution effects (particularly in the weld made with unbuttered joint surfaces), thermal effects, and other factors such as ferrite morphology, dissolution of ferrite, and cooling rate to be discussed shortly. Here, we should also mention possible changes in the amount of nitrogen pickup during welding, which could contribute in part to variations in ferrite content.

The FN associated with various ferrite morphologies is closely related to the volume percent of ferrite and in turn the composition. As discussed earlier, the orientation of the ferrite with respect to surface examined could bring about a minor variation in FN. The FN associated

with each morphology is shown in Fig. 3. For example, the FN for type I vermicular morphology varied from 9 to 12, depending on the section on which the magnetic measurements were made. Although quantitative metallography showed no drastic variations in the volume percent of ferrite for the top and side views, the magnetic measurements showed a definite difference in FN. The same observation was true for type II lacy morphology. Hence the difference in FN seems to be related to the microstructural continuity and the interaction of the magnetic flux with the ferrite.

Dissolution of the ferrite from subsequent thermal cycles in a multipass weld is another factor that could contribute to the variations in ferrite content. Figure 6 shows such a variation in root pass FN for the welds 1 and 2 as a function of seven other subsequent passes. Results show a drastic reduction in root pass FN for both welds with the first three subsequent passes, after which the FN remains constant. An extensive microstructural analysis of the root pass in welds 1 and 2 indicated that the reduction in ferrite results from its dissolution during the thermal excursions of the weld. Chemical extraction from samples of the welds revealed no precipitates. Figure 7 is a transmission electron micrograph of a sample taken from the root pass deposit of weld 1; it shows ferrite in an austenite matrix. No precipitation of any kind was observed at the γ-δ interface or within the delta phase. The observed absence of transformation products is typical of the investigated type 308 stainless steel weld metal only. Transformation of ferrite to sigma from thermal cycle effects in a multipass weld is possible for weld metals of different compositions.

An investigation of the effect of solidification rate on the ferrite content has led to some interesting conclusions. It has been suggested that the increase or decrease in ferrite content of austenitic stainless steel weld metal caused by a decrease or increase in solidification rate, respectively, provides an alternate method other than composition for varying the ferrite content.[29] This variation in ferrite level as a function of solidification rate is closely related to the kinetics of

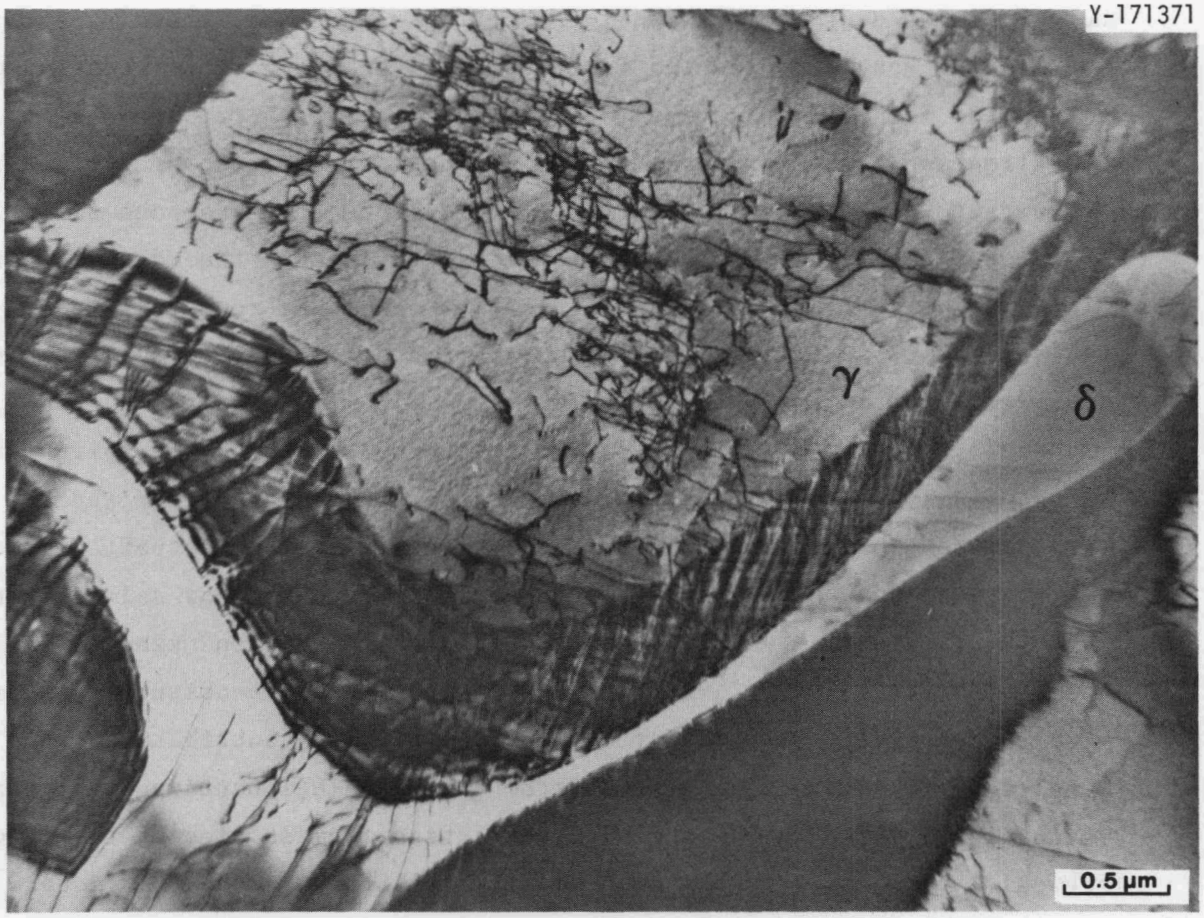

Fig. 7. Transmission electron micrograph showing the absence of transformation products in a sample taken from the root pass of the type 308 stainless steel multipass weld.

primary $\delta \rightarrow \gamma$ transformation. It is a well established fact that the solidification substructure size (primary or particularly secondary dendrite arm spacing) is a strong function of local solidification time θ defined for a point in the weld as the difference in time between the passing of the liquidus and solidus isotherms.[30] Therefore,

$$d = C\theta^{n} (0.3 < n < 0.5) , \qquad (1)$$

where d is the dendrite arm spacing and C is a constant. Thus, the dendrite arm spacing would be finer for high solidification rates and coarser for low solidification rates. The kinetics of primary $\delta \rightarrow \gamma$ transformation depends greatly on the diffusion distances as determined by the dendrite arm spacing. Therefore, avoiding any extreme nonequilibrium situations, the higher the solidification rate (within the realm of normal welding processes), the finer the spacing of the substructure. Hence, a greater amount of primary ferrite would transform to austenite in a given time, resulting in lower ferrite content in the microstructure. The amount of ferrite would be optimum as determined by the effects from the two opposing factors; short time at high temperature and finer spacing of the dendrite substructure. However, postsolidification heat effects do contribute to the $\delta \rightarrow \gamma$ transformation. Similarly, for low solidification rates the solidification substructure would be coarser and hence a large amount of primary ferrite would remain untransformed to austenite. The extent of solute redistribution involved could also contribute to the extent of this reaction via chromium partitioning and buildup within the ferrite, thus contributing to its stability. In addition, all the above could be altered by superposition of postsolidification heat effects.

During the present investigation ferrite measurements on samples solidified at various cooling rates showed very little variation in the ferrite content (Fig. 8). An average FN for each sample was obtained by measuring the FNs on different sections of the sample to avoid effects of orientation. Also, a water-quenched type 308 filler metal droplet had an FN of 6.1 and that of the slowly cooled small ingot sample of the same alloy had an FN of 7.0, as shown in Fig. 8 by the closed circle and triangle, respectively. However, it should be pointed out that in the slowly cooled sample, postsolidification heat effect may have reduced the ferrite content. The role of solidification rate and the associated substructural size in the ferrite dissolution kinetics and hence the ferrite content can be elucidated as follows. Figure 8 shows the change in ferrite content at 1000°C (1832°F) for different times on three samples of type 308 stainless steel filler metal used in this investigation with three different secondary dendrite arm spacings. The rate of change of FN is higher for the

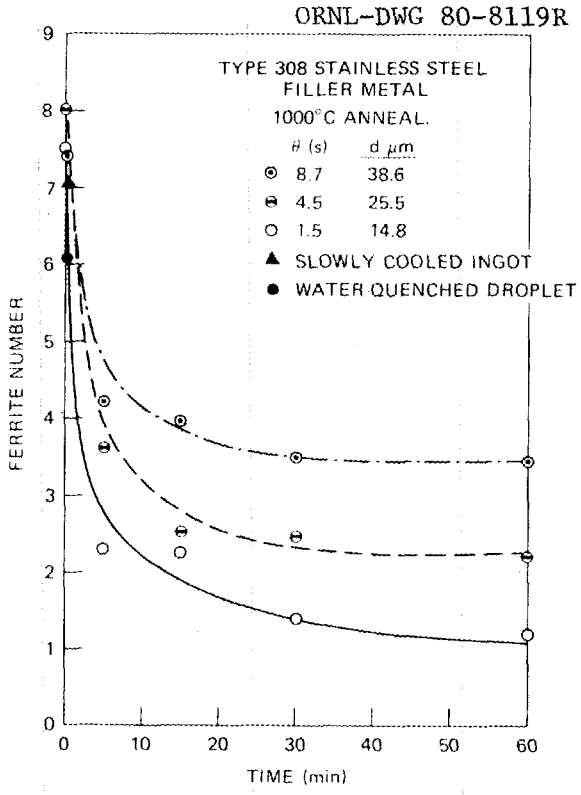

Fig. 8. Effect of heat treatment on the ferrite number in type 308 stainless steel filler metal castings solidified at various cooling rates. θ = local solidification time; d = dendrite arm spacing.

sample with finer dendrite arm spacing than for the one containing coarse dendrite spacings. As discussed earlier this is attributable mostly to the dissolution rate of ferrite being higher in samples containing finer dendrite spacing than in the one having coarser spacing. The structure of a cast type 308 stainless steel sample [secondary dendrite arm spacing of 25.5 μm (1.00 mil)] before and after the 1000°C (1832°F) heat treatment for 900 s is shown in Fig. 9. The arrows indicate evidence of ferrite dissolution. In addition, electrolytic extraction of specimens from these samples revealed $M_{23}C_6$, although the presence of a small amount of sigma could not be ruled out because of its possible dissolution during the extraction procedure.

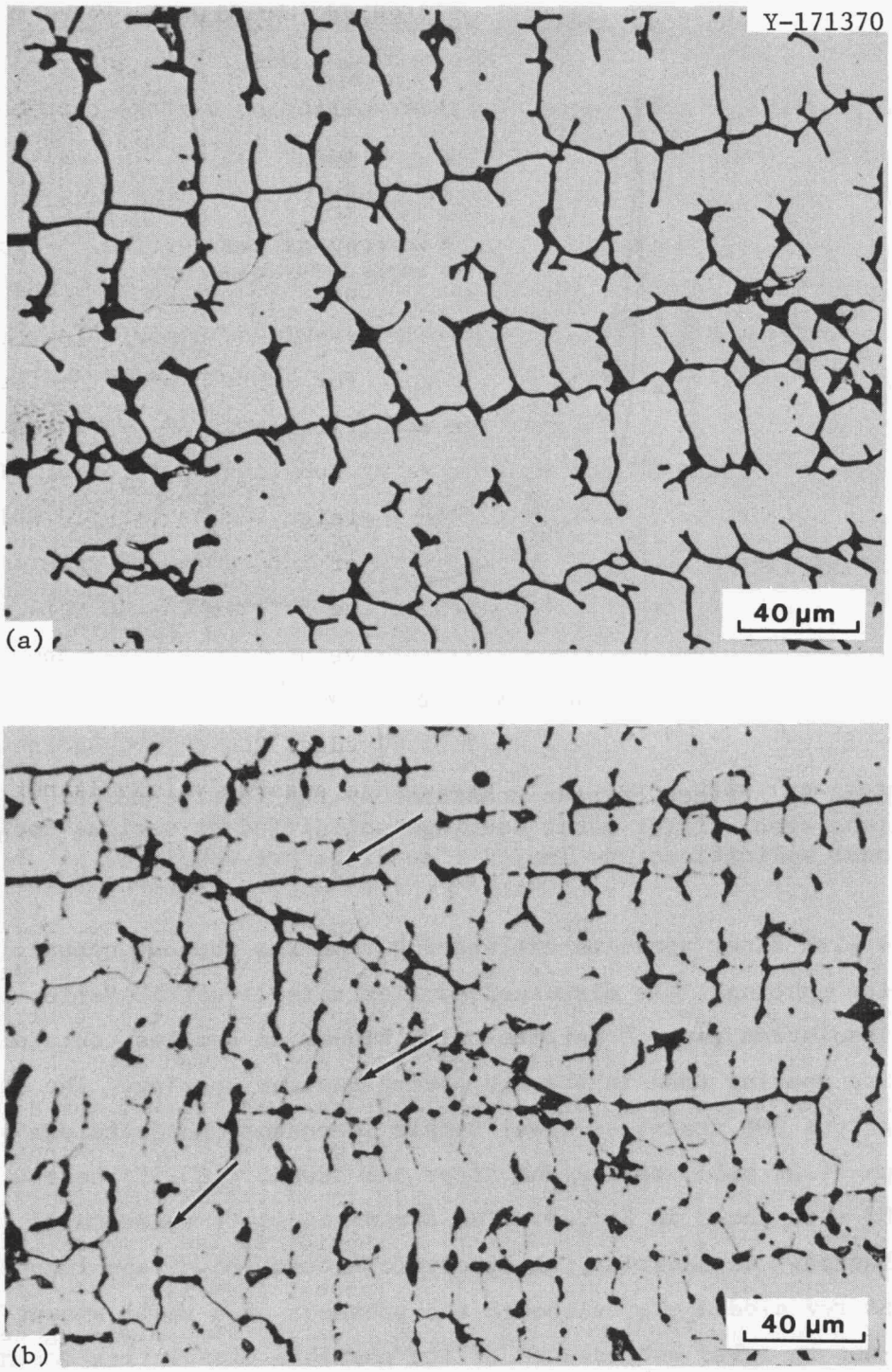

Fig. 9. Type 308 stainless steel filler metal casting [secondary dendrite arm spacing of 25.5 µm (1.00 mil)]. (a) Untransformed ferrite network before heat treatment. (b) Dissolution of ferrite upon heat treatment at 1000°C (1832°F) for 900 s.

SHAPE INSTABILITY OF FERRITE IN THE WELD

To determine the microstructural stability of various ferrite morphologies, four samples containing the morphologies identified earlier were heat-treated for 10 min at 1050°C (1922°F). All the samples showed extensive degradation in the micromorphology of the ferrite. Figure 10 compared with Fig. 3 shows the extent of change in morphology observed in various samples. Figure 10(a) shows the breakdown in morphology of type I ferrite. On exposure to high temperature for short times, the ferrite seems to assume a rugged cylindrical form (with reduced δ-γ interfacial area) and further breaks down into rows of spherical particles. The phenomenon appears very similar to the Rayleigh instability,[31] which describes the breakdown of a liquid cylinder into a row of spherical droplets. It should be pointed out that the ferrite in the weld metal is a nonequilibrium phase and could dissolve at temperatures above the γ-($\sigma + \gamma + \delta$) phase boundary but below the γ-($\gamma + \delta$) solvus. Also, the observed ferrite shape in type I of sharp edges and curved surfaces (γ-δ interface) with large ratio of surface area to volume is not the most stable ferrite morphology. Ferrite of such shape will generally have differences or gradients in chemical potential of the constituent atoms as a result of capillarity.* Therefore, on exposure to high temperatures, two equilibrating processes proceed simultaneously. One is changes in ferrite shape leading to the formation of spherical particles with reduced interfacial area and associated interfacial energy, and the other is dissolution of δ-ferrite. The former process results from the diffusive transport under the driving force of capillarity.[32] The sequence of events that occurs is shown schematically in Fig. 11. The simultaneous dissolution of δ-ferrite adds another dimension to the complexity of treating shape effects quantitatively. Shape instability such as the one described above has been observed in other materials containing duplex structures, particularly eutectics, with one major difference being that the volume fraction of the second phase in the eutectic remains constant.

---

*The effect of curvature of a surface on the chemical potential of surface atoms.

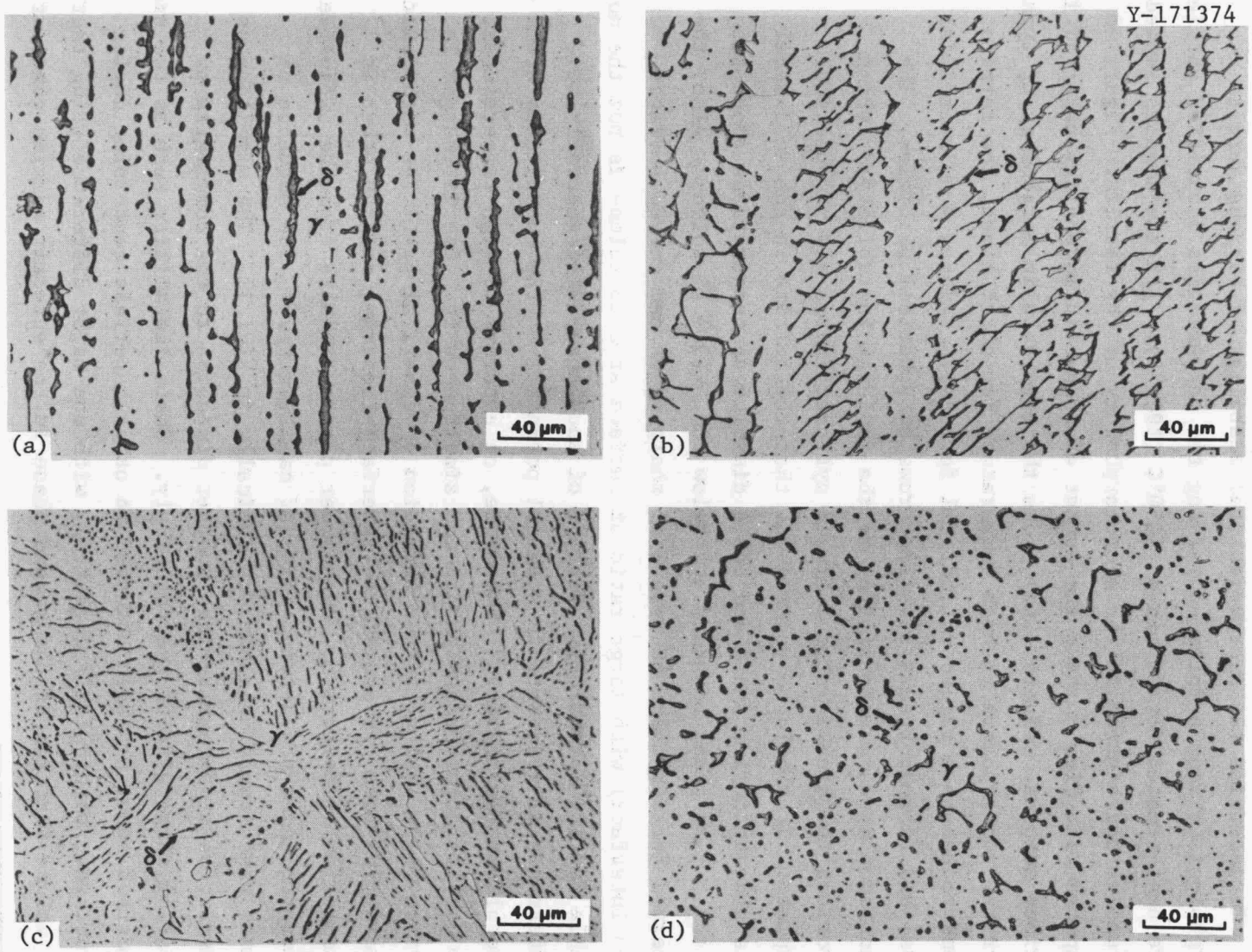

Fig. 10. Shape instabilities in various ferrite morphologies. (a) Type I, vermicular. (b) Type II, lacy. (c) Type III, acicular. (d) Type IV, globular.

ORNL-DWG 80-11932

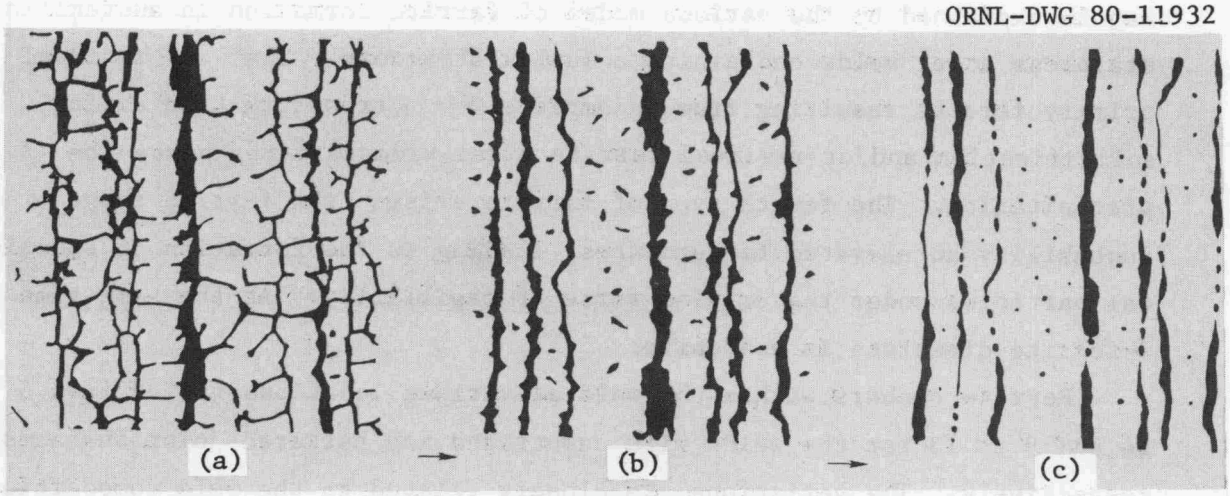

Fig. 11. Sequence of events in the shape instability of ferrite.

The phenomenon has been treated quantitatively by Cline.[28] The morphological instability of type II ferrite on exposure to high temperature is shown in Fig. 10(b). Here the well interlaced ferrite gets disconnected randomly during the dissolution process and sometimes assumes a globular morphology. Given sufficient time this could lead to complete dissolution of ferrite in austenite. Type III ferrite on exposure to high temperature breaks down into rows of well spaced spherical particles, as shown in Fig. 10(c). The problem here again appears to be one of shape instability accompanied by dissolution of ferrite. Finally, when the sample containing type IV ferrite (globular) was exposed, the microstructure changed little except more of the ferrite globules went into solution.

CONCLUSIONS

Four distinct types of ferrite morphologies have been identified in type 308 stainless steel multipass welds, with FNs ranging from 9 to 15: vermicular, lacy, acicular, and globular. The first three types are related to solidification and transformations following solidification. The fourth type is related to the thermal shape instability of any of the other three types of ferrite. The origin of the three types of ferrite

may be explained by the various modes of ferrite formation in austenitic stainless steel welds containing a duplex structure. They are residual primary ferrite resulting from incomplete $\delta \rightarrow \gamma$ transformation during solidification and/or residual ferrite after Widmanstätten austenite precipitation. The fourth type of ferrite arises from ferrite shape instability at elevated temperatures, leading to the formation of spherical particles under the driving force of capillarity. At the same time δ-ferrite dissolves in austenite.

Ferrite numbers within the weld at various locations varied from 5 to 14 and 9 to 13 for the welds with unbuttered and buttered joint surfaces, respectively. The variations are closely related to the weld composition, ferrite morphology, and dissolution of ferrite during thermal cycles experienced by the weld metal from subsequent weld passes. Weld metal solidification rates encountered within the confines of common welding processes may not significantly affect the ferrite content. However, the scale of the solidification substructure associated with various solidification rates may influence the ferrite dissolution or transformation kinetics.

ACKNOWLEDGMENTS

The authors gratefully acknowledge C. J. McHargue, Program Manager, for encouragement and support and V. T. Houchin for welding. We also acknowledge J. W. McEnerney and G. M. Goodwin for technical discussions, J. O. Steigler and C. T. Liu for reviewing the manuscript, S. Peterson for editing, and A. J. Carter for preparing the manuscript for publication.

REFERENCES

1. J. C. Borland and R. N. Younger, "Some Aspects of Cracking in Austenitic Steels," *Br. Weld. J.* 7(1): 22–60 (1960).
2. F. C. Hull, "Effect of Delta Ferrite on the Hot Cracking of Stainless Steel," *Weld. J. (Miami)* 46(9): 399-s–409-s (1967).

3. Y. Arata, F. Matsuda, and S. Katayama, "Solidification Crack Susceptibility in Weld Metals of Fully Austenitic Stainless Steel (Report I) — Fundamental Investigation on Solidification Behavior of Fully Austenitic and Duplex Microstructures and Effect of Ferrite on Microsegregation," *Trans. JWRI* 5(2): 35–51 (1976).

4. W. T. DeLong, "Ferrite in Austenitic Stainless Steel Weld Metal," *Weld. J. (Miami)* 53(7): 273-s–286-s (1974).

5. D. Hauser and J. A. VanEcho, *Properties of Steel Weldments for Elevated Temperature Pressure Containment Applications,* MPC-9, G. V. Smith, ed., American Society of Mechanical Engineers, New York, 1978, pp. 17–46.

6. D. P. Edmonds, D. M. Vandergriff, and R. J. Gray, "Effect of Delta Ferrite Content on the Mechanical Properties of E308-16 Stainless Steel Weld Metal. III. Supplement Studies," pp. 47–61 in *Properties of Steel Weldments for Elevated Temperature Pressure Containment Applications,* MPC-9, The American Society of Mechanical Engineers, New York, 1978.

7. R. Castro and J. J. de Cadenet, *Welding Metallurgy of Stainless and Heat Resisting Steels,* Cambridge University Press, London, 1974.

8. R. Viswanathan, J. I. Nurminen, and R. G. Aspden, "Stress Corrosion Behavior of Stainless Steel Welds in High Temperature Water Containing Chloride," *Weld. J. (Miami)* 58(4): 118-s–126-s (1979).

9. T. M. Devine, "Influence of Ferrite Morphology and Carbon Content on the Sensitization of Duplex Stainless Steel," paper presented at 109th AIME Annual Meeting, Las Vegas, Nev., February 1980.

10. C. L. Estes and P. W. Turner, "Dilution in Multipass Welding AISI 4130 to Type 304 Stainless Steel," *Weld. J. (Miami)* 43(12): 541-s–550-s (1964).

11. G. M. Goodwin, N. C. Cole, and G. M. Slaughter, "A Study of Ferrite Morphology in Austenitic Stainless Steel Weld Metals," *Weld. J. (Miami)* 51(9): 425-s–429-s (1972).

12. N. Suutala, T. Takalo, and T. Moisio, "Relationship Between Solidification and Microstructure in Austenitic and Austenitic-Ferritic Stainless Steel Welds," *Metall. Trans. A* 10A: 512–14 (1979).

13. T. Takalo and T. Moisio, "Single Phase Ferritic Solidification Mode in Austenitic-Ferritic Stainless Steel Welds," *Metall. Trans. A* 10A: 1183–90 (1979).

14. J. K. Lai, B. Nath, and R. D. Townsend, "Variations in Delta-Ferrite Content and Morphology in a Multipass Type 316 Weldment and Their Effect on Creep Rupture Properties," paper presented at British Nuclear Energy Society Conference on Welding and Fabrication in the Nuclear Industry, London, April 1979.

15. T. Takalo and T. Moisio, "Influence of Ferrite Content on its Morphology in Some Austenitic Weld Metals, *Metall. Trans. A* 7A: 1591–92 (1976).

16. S. L. Schaeffler, "Constitution Diagram for Stainless Steel Weld Metal," *Met. Prog.* 56: 680 and 680 B (1949).

17. W. T. DeLong, G. Ostrom, and E. Szumachowski, "Measurement and Calculation of Ferrite in Stainless Steel Weld Metal," *Weld. J. (Miami)* 35(11): 526-s–533-s (1956).

18. C. J. Long and W. T. DeLong, "The Ferrite Content of Austenitic Stainless Steel Weld Metal," *Weld. J. (Miami)* 52(7): 281-s–297-s (1973).

19. S. A. David and J. M. Vitek, "Solidification Behavior and Microstructural Analysis of Austenitic Stainless Steel Laser Welds," paper presented at the AIME Meeting, Chicago, Ill., February 1981; to be published in the proceedings.

20. S. A. David and H. D. Brody, "Controlled Solidification of Peritectic Alloys," pp. 144–51 in *Proc. Int. Conf. Solidification,* Metals Society, London, 1979.

21. Private communication, H. D. Brody, University of Pittsburgh, Pa., to S. A. David, June 1980.

22. J. I. Nurminen and H. D. Brody, "Dendrite Morphology and Microsegregation in Titanium Base Alloys," pp. 1893–914 in *Titanium Sci. Technol. Proc. Int. Conf. 2nd,* Vol. 3, R. I. Jaffee and H. M. Burte, eds., Plenum, New York, 1973.

23. Private communication, S. Kou, Carnegie Mellon University, Pittsburgh, Pa., to S. A. David, October 1980.

24. J. M. Leitnaker, G. A. Potter, R. H. Shannon, D. P. Edmonds, R. S. Crouse, K. F. Russell, and C. W. Houck, *Transformations Occurring on Aging of 16-8-2 Weld Metal,* ORNL-5400 (June 1978).

25. S. A. David, G. M. Goodwin, and D. N. Braski, "Solidification Behavior of Austenitic Stainless Steel Filler Metals," *Weld. J. (Miami)* 59(11): 330-s–336-s (1979).

26. J. C. Lippold and W. F. Savage, "Solidification of Austenitic Stainless Steel Weldments: Part I — A Proposed Mechanism," *Weld. J. (Miami)* 59(12): 362-s–374-s (1979).

27. M. C. Flemings, *Solidification Processing,* McGraw-Hill, New York, 1974, p. 229.

28. H. E. Cline, "Shape Instabilities of Eutectic Composites at Elevated Temperatures," *Acta Metall.* 19: 481–90 (1971).

29. Personal communication, C. D. Lundin, University of Tennessee, Knoxville, to S. A. David, December 1977.

30. H. D. Brody and S. A. David, "Application of Solidification Theory to Titanium Alloys," pp. 21–34 in *Proc. Science Technology and Application of Titanium,* R. Jaffee and N. Promisel, eds., Pergamon, New York, 1970.

31. J. W. Strelt (Lord Rayleigh), *London Math. Soc. Proc.* 10: 4 (1879).

32. W. W. Mullins, "Metal Surfaces," *ASM Trans. Q.* 56: 17–66 (1963).

ORNL/TM-7810
Distribution
Category UC-25

INTERNAL DISTRIBUTION

1–2. Central Research Library
3. Document Reference Section
4–5. Laboratory Records Department
6. Laboratory Records, ORNL RC
7. ORNL Patent Section
8. V. B. Baylor
9. C. R. Brinkman
10. R. S. Crouse
11–15. S. A. David
16. D. P. Edmonds
17. G. M. Goodwin
18–22. C. P. Haltom
23. J. P. Hammond
24–28. S. E. Hanzelka
29–31. M. R. Hill
32. J. A. Horak
33. R. L. Klueh
34. P. J. Maziasz
35. R. E. McDonald
36. C. J. McHargue
37. R. K. Nanstad
38. H. E. Reesor
39. P. L. Rittenhouse
40. J. L. Scott
41. V. K. Sikka
42. G. M. Slaughter
43. J. O. Stiegler
44. R. W. Swindeman
45. P. A. Tortorelli
46. J. M. Vitek
47. C. L. White
48. F. W. Wiffen
49. R. O. Williams
50. A. L. Bement, Jr. (Consultant)
51. E. H. Kottcamp, Jr. (Consultant)
52. Alan Lawley (Consultant)
53. T. B. Massalski (Consultant)
54. R. H. Redwine (Consultant)
55. A. D. Rossin (Consultant)

EXTERNAL DISTRIBUTION

56–62. DOE, DIVISION OF MATERIALS SCIENCES, Washington, DC 20545

R. J. Gottschall
L. C. Ianniello
J. S. Kane
F. V. Nolfi
D. K. Stevens
M. C. Wittels
S. Wolfe

63. DOE, OAK RIDGE OPERATIONS OFFICE, P.O. Box E, Oak Ridge, TN 37830

Office of Assistant Manager for Energy Research and Development

64–271. DOE, TECHNICAL INFORMATION CENTER, OFFICE OF INFORMATION SERVICES, P.O. Box 62, Oak Ridge, TN 37830

For distribution as shown in TID-4500 Distribution Category, UC-25 (Materials)

☆U.S. GOVERNMENT PRINTING OFFICE: 1981-740-062/153